

A Numerical Study on Liquid Mixing in Multichannel Micromixers

Yuanhai Su,^{†,‡} Anna Lautenschleger,[†] Guangwen Chen,[‡] and Eugeny Y. Kenig^{*,†}

[†]Chair of Fluid Process Engineering, Faculty of Mechanical Engineering, University of Paderborn, D-33098, Paderborn, Germany

[‡]Dalian National Laboratory for Clean Energy, Dalian Institute of Chemical Physics, Chinese Academy of Sciences, Dalian 116023, China

ABSTRACT: Single microchannels and their arrangements for liquid mixing are investigated numerically. A smaller lateral inlet diameter and the zigzag form of the channels are found to be beneficial for the mixing performance in microchannels. Under proper operational conditions, the mixing process can be almost completed. Furthermore, some constructal distributor designs for the arrangement of microchannels are proposed and analyzed with regard to the fluid distribution. For the optimized distributor, the standard deviation from perfectly even distribution does not exceed 4% while keeping the pressure drop low. Two multichannel micromixer designs are suggested, with accordingly optimized microchannels and distributors, and their mixing performance is very close to that of a single microchannel. The specific energy dissipation in the multichannel micromixer is in the range of 0.016–93 W/kg, which is similar to batch reactors. Finally, the design procedure for multichannel micromixers is proposed.

1. INTRODUCTION

Mixing processes in liquid–liquid systems are widespread in the process industry. They comprise macro- and mesomixing (coarse-scale phenomena), and micromixing that occurs on molecular scale. In many unit operations, for example, precipitation,¹ crystallization,^{2,3} polymerization,⁴ self-catalysis,⁵ and enzymatic catalysis,⁶ the mixing efficiency represents a decisive factor, whereas an optimized mixing performance improves the contact of reactants and greatly influences selectivity, yield, and quality of products. In particular, the mixing performance may control the molecular weight distribution in polymerization. Recent progress in reactor design yielding better mixing efficiency has been remarkable. Impinging flow reactors,⁷ rotating packed bed reactors,^{8,9} static mixers with internal baffles,¹⁰ and micromixers¹¹ demonstrate outstanding progress in reactor design.

During the last two decades, chemical engineering has experienced a spectacular trend toward microscale applications. This represents one of the most important areas in the process intensification concept. The microscale applications benefit from the miniaturization of the unit-building channels in which the characteristic lengths reach the values typical for boundary layers.^{12–14} A number of micromixers and microreactors have been designed, attracting increasing attention of both industry and academia.^{15–21} Furthermore, a considerable variety of novel micromixer concepts have been proposed, such as interdigital micromixer,²² split-and-recombine micromixer,²³ micromixer based on the collision of microsegments,²⁴ multifunctional micromixer, which makes use of alternating current electroosmotic flow and asymmetric electric field,²⁵ packed-bed microreactors,^{18,26,27} etc. However, because of their complex structures, manufacturing of these micromixers is difficult, and their practical application is limited. In contrast, T-shaped microchannel mixers are easy to design and manufacture; hence they are widely used for laboratory tasks and have high potential for industrial application.

Many research groups investigated hydrodynamics and mixing in microchannels by numerical and experimental methods. Engler et al.²⁸ had revealed that there were three

different laminar flow regimes inside the junction of a T-shaped microchannel, depending on the Reynolds number, stratified flow, vortex flow, and engulfment flow. It was found that the vortices inside a T-shaped microchannel with a rectangular cross-section occurred even at low Reynolds numbers and they were beneficial to the mixing performance improvement. Adeosun and Lawal²⁹ used residence time distribution (RTD) to characterize the flow and mixing in a T-shaped microchannel by computational fluid dynamics (CFD) simulations and UV–vis absorption spectroscopy detection technique for experimental validation. Their numerical and experimental results were in good agreement, demonstrating that CFD simulations could be used as a predictive tool in the design and optimization of microchannels.

It is well-known that the geometrical structures of reactors and mixers affect the hydrodynamics and, consequently, the mixing performance. Hong et al.³⁰ carried out a numerical analysis of mixing in an innovative microchannel with modified Tesla structures over a wide range of flow rates. It was found that these structures were advantageous for mixing at higher flow rates, and the mixing performance was influenced by both diffusion and chaotic advection caused by the Tesla structures. Chang and Cho³¹ designed and fabricated a microchannel with alternating whirls and laminations. This design was found to be capable of establishing repeated rotational flow fields that could mix fluids in a wide range of flow rates. Mengeaud et al.³² numerically studied the mixing process in a zigzag microchannel with a “Y” inlet junction. They demonstrated the effects of both flow rate and channel geometry on hydrodynamics and mixing efficiency. Below the critical Reynolds number, the effect of the zigzag configuration on hydrodynamics was found to be negligible, and mixing was entirely dominated by molecular diffusion, while the diffusion distance

Received: June 18, 2013

Revised: November 22, 2013

Accepted: December 2, 2013

Published: December 2, 2013

was of primary importance. For higher Reynolds numbers, the recirculation of the laminar flow in the zigzag configuration contributed to mixing, and this effect increased for small diffusion coefficients. Ansari and Kim³³ performed a numerical study of the mixing of fluids in a microchannel with circular mixing chambers. It was demonstrated that the presence of a flow recirculation zone in the circular chamber resulted in enhanced mixing, especially for larger Reynolds numbers, and higher mixing efficiency was associated with larger pressure drop. Soleymani et al.³⁴ carried out a numerical investigation of liquid mixing in T-shaped microchannels. Their simulation results showed that the occurrence and development of vortices in the T-junction of the microchannel were essential for a good mixing performance, strongly depending on the flow rate and the geometrical parameters of the microchannel (e.g., aspect ratio and angle between two inlet channels).

In addition to excellent mixing performance, the micro-reaction technology has another advantage, in that it is easy to realize the increase in the throughput via the numbering-up approach. However, maintaining the mixing and reaction characteristics of single microchannels during numbering-up is not trivial. One of the important issues that should be considered with care is a good fluid distribution of different fluids among parallel microchannels. This requires properly designed fluid distributors. Saber et al.³⁵ demonstrated that controlling the flow uniformity in parallel channels could result in an improvement of the overall reaction selectivity, while reducing simultaneously the overall pressure drop. Commenge et al.³⁶ investigated the specific features of fluid flow through a multiplate microchannel reactor by an approximate pressure drop model validated by comparison with numerical simulations. Amador et al.³⁷ investigated the effects of manufacturing tolerances and channel blockage on the flow distribution in multichannel micromixers with different structures by a method based on the theory of electrical resistance network. This method was further verified by numerical simulations and could be used for predicting the flow distribution in multichannel micromixers. Yue et al.³⁸ demonstrated that the integration of constructal distributors into multichannel micromixers could ensure flow uniformity and almost keep the mass transfer performance for gas–liquid two-phase system as high as that achieved in a single microchannel. This conclusion was drawn from experiments in a relatively wide operational range during the numbering-up process.

In liquid mixing processes, the understanding of the design parameters for the arrangement of single microchannels (ASMC) is still insufficient. The main objective of this study is to carry out a thorough numerical analysis of liquid mixing in multichannel micromixers. The effect of the shape and size of the inlet, as well as of the structure of the mixing channel on the mixing efficiency in single microchannels, is investigated. Flat constructal distributor designs for ASMC are suggested, and fluid distribution and pressure drop are characterized. Furthermore, two multichannel micromixer designs are proposed with microchannels and distributors, and their mixing performance is studied numerically. Finally, the ASMC effect and energy dissipation in the multichannel micromixer are evaluated.

2. MULTICHANNEL MICROMIXER AND SINGLE MICROCHANNEL DESIGNS

High throughput microreactor systems are based on ASMC for parallel operation. Figure 1 shows the structure and details of such an arrangement. A distributor for the first liquid is placed on one side of a plate.³⁹ Parallel single microchannels are fabricated and connected to this distributor on the same side.

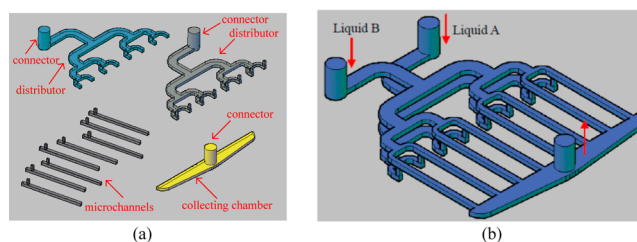


Figure 1. Multichannel micromixer design: components (a), assembly (b).

Another distributor for the second fluid is placed on the other side of the plate, while its outlets are also connected to the parallel microchannels. The single microchannels and the distributors represent the decisive components of the multichannel micromixer. In this study, they are thoroughly investigated to obtain optimized multichannel micromixer design.

From the manufacturing point of view, single microchannels with the cross-flowing inlet configuration are very easy to assemble in ASMC. For such inlet configuration, the angle between lateral and longitudinal inlets is fixed at 90°, while the size and shape of the lateral inlet, as well as the structure of the mixing channel, are varied, as shown in Figure 2.

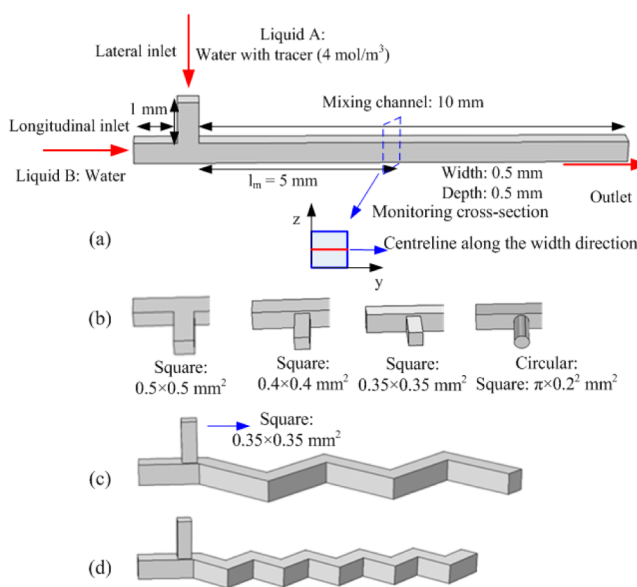


Figure 2. (a) Schematic diagram of the T-shaped microchannel; (b) inlet configurations with different size and shape; (c) microchannel with four zigzag-form structures; and (d) microchannel with nine zigzag-form structures.

3. SINGLE MICROCHANNEL ANALYSIS

3.1. Governing Equations and Calculation of Mixing Efficiency. The mixing process of two miscible liquids in single microchannels is investigated numerically. Liquid A (water with tracer) and liquid B (water) with the volumetric ratio of 1 are fed into the mixing channel. These liquids contact each other at the microchannel inlet junction. The mixing process occurs within the microchannel, and the tracer approaches an even distribution. The governing equations describing the phenomena in microchannels are the continuity, momentum (Navier–Stokes), and the mass transport equations:

$$\nabla \cdot u = 0 \quad (1)$$

$$\frac{\partial u}{\partial t} + u \cdot \nabla u = -\frac{1}{\rho} \nabla p + \nu \nabla^2 u \quad (2)$$

$$\frac{\partial c}{\partial t} + (u \cdot \nabla) c = D \nabla^2 c \quad (3)$$

where u is velocity vector, p is pressure, ν is kinematic viscosity of water, c is concentration of the tracer in the liquid, and D is the molecular diffusion coefficient of the tracer in water, which is assumed to be $2 \times 10^{-9} \text{ m}^2/\text{s}$ in our simulations (diffusion coefficients of various solutes in liquids are usually in the range of 10^{-10} – $10^{-8} \text{ m}^2/\text{s}$). The no-slip boundary condition is applied to all channel walls, the velocity and concentration values are preset at the inlets, and atmospheric pressure is assumed at the outlet. The numerical solution of eqs 1–3 provides pressure, velocity, and concentration distributions. It is obtained with the help of the commercial tool COMSOL Multiphysics⁴⁰ based on the finite element method. The concentration field (scalar field) can further be used to evaluate the mixing performance at an arbitrary cross-section of the microchannel. The mixing efficiency (α) is calculated as follows:²⁸

$$\alpha = 1 - \sqrt{\frac{\sigma_M^2}{\sigma_{\max}^2}} \quad (4)$$

where σ_{\max}^2 is the square of the maximum possible variance of the tracer concentration, and σ_M^2 is defined by the following equation:

$$\sigma_M^2 = \frac{1}{n} \sum_{i=1}^n (c_i - \bar{c}_M)^2 \quad (5)$$

Here, n is the number of sampling points inside the monitoring cross-section, c_i is the concentration at point i , and \bar{c}_M is the optimal mixing concentration of the tracer when the mixing process is completed. When the number of sampling points (n) is large enough, eq 4 can be replaced by the following equation:

$$\begin{aligned} \alpha &= 1 - \sqrt{\frac{\int_S (c_i - \bar{c}_M)^2 ds/S}{\int_S (c_{\text{unmix}} - \bar{c}_M)^2 ds/S}} \\ &= 1 - \sqrt{\frac{\int_S (c_i - \bar{c}_M)^2 ds/S}{\sigma_{\max}^2}} \end{aligned} \quad (6)$$

where S is the area of the monitoring cross-section, and c_{unmix} is the tracer concentration when the mixing process of the two liquids is infinitely slow. In eq 6, $\alpha = 0$ indicates no mixing, whereas $\alpha = 1$ corresponds to complete mixing. In this way, the mixing performance in microchannels can be characterized on the basis of numerical simulations of the tracer concentration field. To obtain the overall mixing efficiency of the microchannel, the outlet of the microchannel is chosen as the monitoring cross-section. Reynolds number used as the main parameter is defined as follows:

$$Re = \frac{\rho u_m d_e}{\mu} \quad (7)$$

$$d_e = \frac{4S}{2(h+w)} \quad (8)$$

3.2. Grid Independence Test and Validation. Tetrahedral grids of different size are exploited for calculating the

velocity and concentration fields in microchannels to ensure the grid size independence of the simulation results. For example, the concentration profiles in the centerline of the monitoring cross-section along the width direction of the T-shaped microchannel, shown in Figure 2a, are investigated. The concentration profiles for both studied Reynolds numbers hardly vary when the grid node number reaches approximately 5×10^6 . For instance, at a Reynolds number of 300, the difference between the mixing efficiencies calculated with 3 840 000 grid points and 5 020 000 grid points is less than 5%. For the grid node number of 5×10^6 , the grid Peclet number ($Pe_\Delta = U\Delta\chi/D$) is in the range 75–2600, depending on the velocity magnitude (0.01–0.3 m/s).

An additional test of our simulations was performed for the mixing process reported by Sullivan et al.⁴¹ Figure 3 shows the

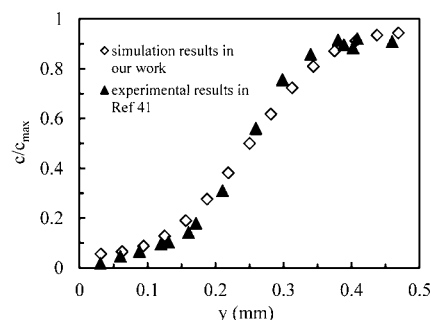


Figure 3. Comparison of simulated normalized concentrations (c/c_{\max}) with experimental values from Sullivan et al.⁴¹

comparison between simulated and experimental normalized concentration profiles along the width direction of the microchannel in the monitoring cross-section. It can be seen the simulation results are in close agreement with the experimental data.

3.3. Effect of Microchannel Inlet Form. A study is carried out with regard to the effects of the size and shape of the lateral inlet on the mixing performance of the microchannels. The results shown in Figure 4a clearly demonstrate that a smaller inlet leads to a higher mixing efficiency under the same flow rate conditions. Higher superficial velocity and momentum can be obtained with a smaller lateral microchannel inlet at the same volumetric flux, as this is beneficial to the penetration of the lateral fluid (liquid A) into another fluid (liquid B) and improves the mixing process in the inlet zone. As shown in Figure 4b, the two microchannels with different lateral inlet shapes (square and circular cross-sections) provide almost the same mixing performance for $Re < 200$. The reason is that the flow remains strictly stratified and the fluid from the lateral inlet cannot penetrate into the second fluid. However, the mixing efficiency in the microchannel with a square cross-section inlet is somewhat higher as compared to the mixing efficiency in the microchannel with a circular cross-section inlet, when the Reynolds number exceeds 200. The perimeter of the lateral inlet with a square cross-section is larger than that with a circular cross-section for the same cross-sectional area ($4\sqrt{S_{\text{in}}} > 2\pi(S_{\text{in}}/\pi)^{1/2}$, where S_{in} is the cross-sectional area of the lateral inlet), so that the lateral inlet with a square cross-section provides more interfacial area when the two fluids interact in the inlet zone of the microchannel.

3.4. Effect of Mixing Channel Form. The zigzag form or the curved form of the channels can improve the liquid mixing process due to the occurrence of secondary flow patterns

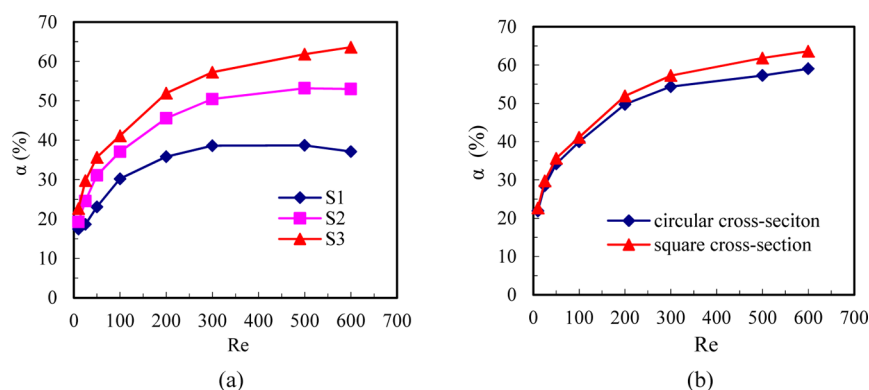


Figure 4. Effects of the size and shape of the lateral inlet on the mixing performance of microchannel 3: square cross-section, $S1 = 0.5 \times 0.5 \text{ mm}^2$, $S2 = 0.4 \times 0.4 \text{ mm}^2$, $S3 = 0.35 \times 0.35 \text{ mm}^2$ (a); circular cross-section and square cross-section ($S = \pi \times 0.2^2 = 0.35 \times 0.35 \text{ mm}^2$) (b).

(Dean vortices) under the action of centrifugal force.^{42,43} The secondary flow promotes rotation of fluid elements in the cross-sections of the curved microchannels and continuously changes along the flow direction, which in turn results in the occurrence of chaotic advection and enhances the stretching and folding of the fluid elements, thus intensifying the mixing process.^{44,45}

Figures 5 and 6 compare the mixing performance in the straight and in the zigzag-form microchannels, while keeping the inlet size and shape as well as the length of the mixing channel constant. It can be seen that the zigzag-form structures can dramatically enhance the mixing efficiency in microchannels, and the mixed liquids almost reach homogeneity ($\alpha = 98\%$) at a Reynolds number of 200 for the microchannel with nine zigzag-form structures. At low Reynolds number (e.g., $Re = 10$), the two miscible fluids flow side-by-side, and the streamlines are hardly interwoven in both straight and zigzag-form microchannels; thus the concentration distribution across the cross-section of the mixing channel is very nonuniform (Figure 5a). In this case, the mixing performance in the zigzag-form microchannels is similar to that in the straight microchannel. Mengeaud et al.,³² who carried out 2D simulations to investigate the mixing process in a zigzag-form microchannel with a Y-shaped inlet junction, reported analogous results.

As shown in Figure 5b, liquid A penetrates into liquid B and forms a flow pattern surrounded by liquid B in the straight microchannel when the Reynolds number further increases (e.g., $Re = 100$). Such contact of two liquids increases the interfacial area, and thus enhances the mixing process in the straight microchannel. However, the streamlines of different liquids are hardly curved and just directly follow the shape of the mixing channel. Under such conditions, mixing is mainly based on molecular diffusion, and the effect of convection is not significant. In contrast to the straight microchannel, the two fluids in zigzag-form microchannels interweave and shear each other due to the impact of zigzag-form structures. More exactly, the fluid elements are stretched, folded, and sheared, and then thinner striation thickness and larger specific interfacial area for mass transport are generated. It can further be predicted that the zigzag-form structures promote the occurrence of chaotic advection in the microchannels. This is illustrated by the corresponding streamline plots and the contours of concentration magnitude in the zigzag-form microchannels (Figure 5b).

In the steady flow regime, to generate chaotic advection for mixing process enhancement, three-dimensional multilayer channels or complicated structures are usually required to stretch and fold the fluid elements.⁴⁶ The zigzag-form microchannels in

the present study can be considered as simple devices, in which the chaotic advection can be generated. Moreover, the microchannel with four zigzag-form structures can nearly provide the same mixing performance as the microchannel with nine zigzag-form structures at relatively high Reynolds number ($Re = 200$), and the effect of the number of the zigzag-form structures on the mixing performance is relatively weak (Figure 6).

On the basis of the simulation results and the aforementioned analysis, it is clear that the mixing process in the microchannels with zigzag-form structures is determined by different mechanisms. When $Re < 10$, the mixing process is dominated by molecular diffusion, and the effects of zigzag-form structures on the mixing efficiency can be neglected. In the region $10 < Re < 100$, it is controlled by both diffusion and convection. In the region $Re > 100$, the mixing process is mainly controlled by chaotic advection. It is worth noting that the flow in the zigzag-form microchannels tends to become unsteady, as the Reynolds number further increases and exceeds 400.

3.5. Pressure Drop Characteristics in Microchannels.

Usually, improved mixing performance in microchannels is reached at the expense of the increased pressure drop (ΔP). Figure 7 shows the pressure drop in the different microchannel structures presented above. This pressure drop is equal to the pressure difference between the lateral inlet and the outlet. The size and shape of the lateral inlet insignificantly influence the pressure drop in T-shaped straight microchannels (Figure 7a). Therefore, the microchannel with a smaller square cross-section of the lateral inlet can be chosen to yield higher mixing efficiency. Dreher et al.⁴⁷ reported that the flow in a straight T-shaped micromixer with $0.3 \times 0.6 \text{ mm}$ rectangular cross-section and 4 mm length mixing channel becomes unsteady at a Reynolds number of about 240. However, in our work, the flow in the straight microchannels remains steady even when the Reynolds number reaches 600. This could also be confirmed by the pressure drop characteristics. When the entrance effect of the inlet zone is eliminated, the pressure drop agrees well with the values predicted by the conventional laminar flow theory.

As shown in Figure 7b, the zigzag-form structures result in a much higher pressure drop as compared to the straight channel, when $Re > 100$ (the chaotic advection region for zigzag-form microchannels), and this phenomenon is especially remarkable for the microchannel with nine zigzags. Actually, in addition to the pressure drop caused by the wall friction effect, the zigzag-form structures significantly increase pressure drop by changing the flow direction and the magnitude of the velocity vector. The impinging of fluids on the microchannel walls where

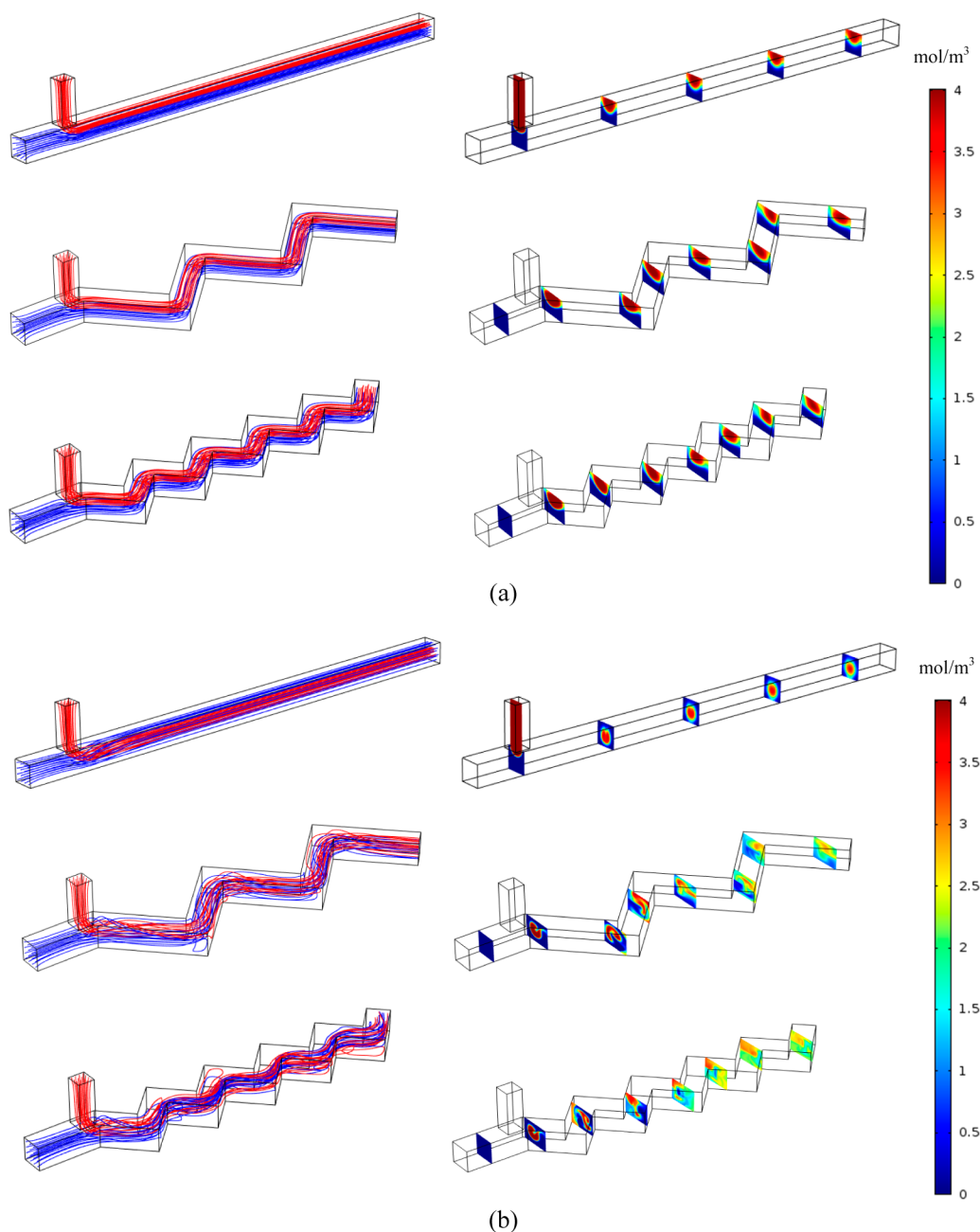


Figure 5. Streamline plots and corresponding contours of concentration magnitude in different microchannels for different Reynolds numbers: (a) $Re = 10$ and (b) $Re = 100$.

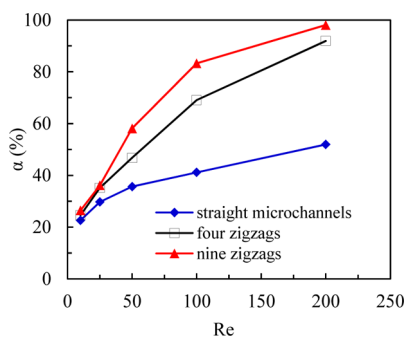


Figure 6. Effect of mixing channel form on the mixing efficiency of microchannels.

zigzag-form structures are positioned also induces pressure drop, and this effect increases with growing flow rate. Therefore, the number of the zigzags and the mixing performance should be considered simultaneously for the optimal design, especially for relatively high Reynolds numbers ($Re > 100$).

4. MULTICHANNEL MICROMIXER ANALYSIS

4.1. Distributor Designs for Multichannel Micromixers. The distributors with manifold structures (e.g., consecutive and bifurcation configuration) are usually applied to distribute the fluids between the parallel microchannels. The use of the bifurcation configurations provides better flow uniformity as compared to the consecutive configurations.^{37,48} In this section, flat constructal distributors with bifurcation

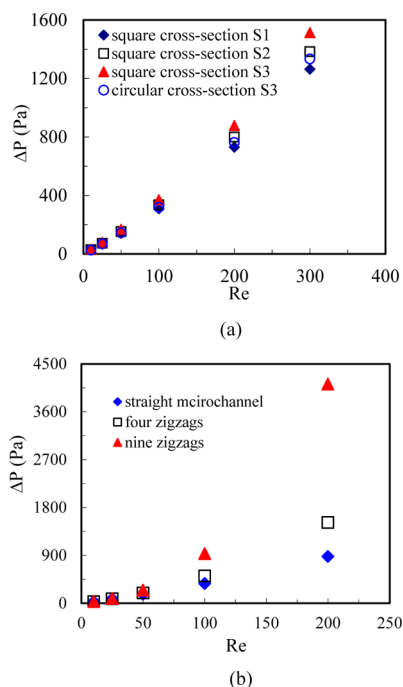


Figure 7. Pressure drop in different microchannel structures: effects of the size and shape of the lateral inlet in T-shaped straight microchannels (a), and effects of zigzag-form structures (b).

configurations (dichotomic tree structures) are designed to obtain good distribution of liquid streams. The structure of distributors comprises three generations (Figure 8a). In the first generation, the inlet channel is split perpendicularly into two opposing channels, and then these two channels are further split into two channels in the second generation. This bifurcation process goes on, finally resulting in $2^3 = 8$ outlets of the distributor. The resulting channels in this bifurcation process have either sharp corners (Figure 8a) or rounding ones (Figure 8b); besides, their length may be different (cf., Figure 8c). To describe the specific geometry of these distributors, the whole distributor structure is subdivided into four zones (shown in Figure 8b). Table 1 summarizes the dimensions of these four zones for different distributors.

CFD simulations are carried out to characterize the fluid distribution in these constructal distributors with the inlet flow rate lower than 1.6 m/s (laminar flow everywhere within the distributors). Continuity and Navier–Stokes equations (eqs 1 and 2) are solved with the commercial tool COMSOL Multiphysics. Figure 9 shows the contours of velocity magnitude evaluated on the central plane of the distributors for two different Reynolds numbers. It can be seen that the velocity field in all zones is fully developed and laminar. It shows axial symmetry at the downstream position of every split point for all distributors when the inlet Reynolds number is low ($Re_{in} = 50$, Figure 9a). In this case, the structure of the constructal distributors has no influence on the fluid distribution, and the uniformity in the eight outlets of each distributor is achieved. For relatively large inlet Reynolds number ($Re_{in} = 600$), the axial symmetry of the velocity field disappears and the fluid cannot be equally distributed at the split points (Figure 9b). These phenomena are more pronounced for distributors 1 and 2, where the distance between the split point and the next split point (l_2) in zones 1–3 for the flow development is shorter than that in distributor 3. For quantification of the flow nonuniformity in these distributors, the

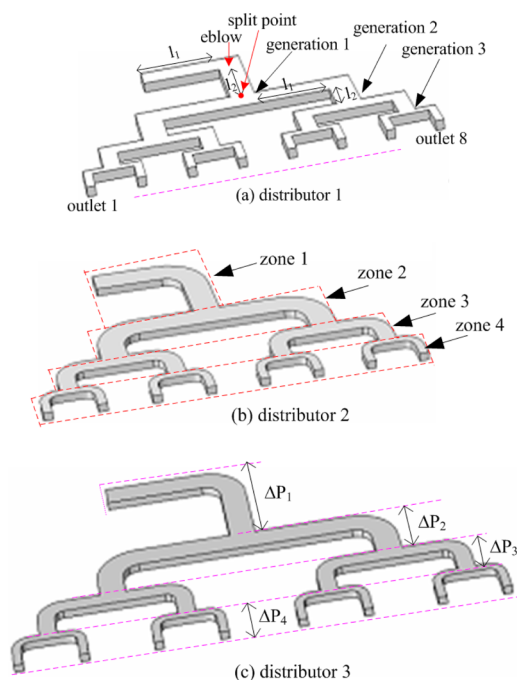


Figure 8. Schematic diagram of constructal distributors with different structures and dimensions.

Table 1. Structures and Dimensions of Constructal Distributors

distributor		w (mm)	l_1 (mm)	l_2 (mm)	depth (mm)	structure of elbow
distributor 1	zone 1	1.5	4.8	4	0.5	right angle
	zone 2	1.5	4.4	2	0.5	right angle
	zone 3	1	1.7	1.5	0.5	right angle
	zone 4	0.5	0.73	1.5	0.5	right angle
distributor 2	zone 1	1.5	3.8	3	0.5	circular arc
	zone 2	1.5	3.4	1	0.5	circular arc
	zone 3	1	1.2	1	0.5	circular arc
	zone 4	0.5	0.23	1	0.5	circular arc
distributor 3	zone 1	1.5	5.66	4.5	0.5	circular arc
	zone 2	1.5	5.48	1.5	0.5	circular arc
	zone 3	1	2.18	1.5	0.5	circular arc
	zone 4	0.5	0.59	1.5	0.5	circular arc

relative deviation (RD_i) and the standard deviation (SD) between the actual velocity magnitude at each outlet and the average velocity value for all eight outlets at uniform distribution are defined as follows:

$$RD_i = \frac{u_i - u_m}{u_m} = \frac{u_i - \frac{1}{8} \sum_{i=1}^8 u_i}{\frac{1}{8} \sum_{i=1}^8 u_i} \quad (9)$$

$$SD = \sqrt{\frac{1}{n-1} \sum_{i=1}^n \left(\frac{u_i}{u_m} - 1 \right)^2} = \sqrt{\frac{1}{7} \sum_{i=1}^8 \left(\frac{u_i}{u_m} - 1 \right)^2} \quad (10)$$

Figure 10 shows the velocity magnitude and RD_i at each outlet of distributor 2 for different Reynolds numbers. It can be seen that the flow uniformity can be nearly reached in the studied constructal distributors at low inlet Reynolds number ($RD_i < 3\%$ when $Re_{in} < 200$), and the nonuniformity increases with increasing inlet Reynolds number.

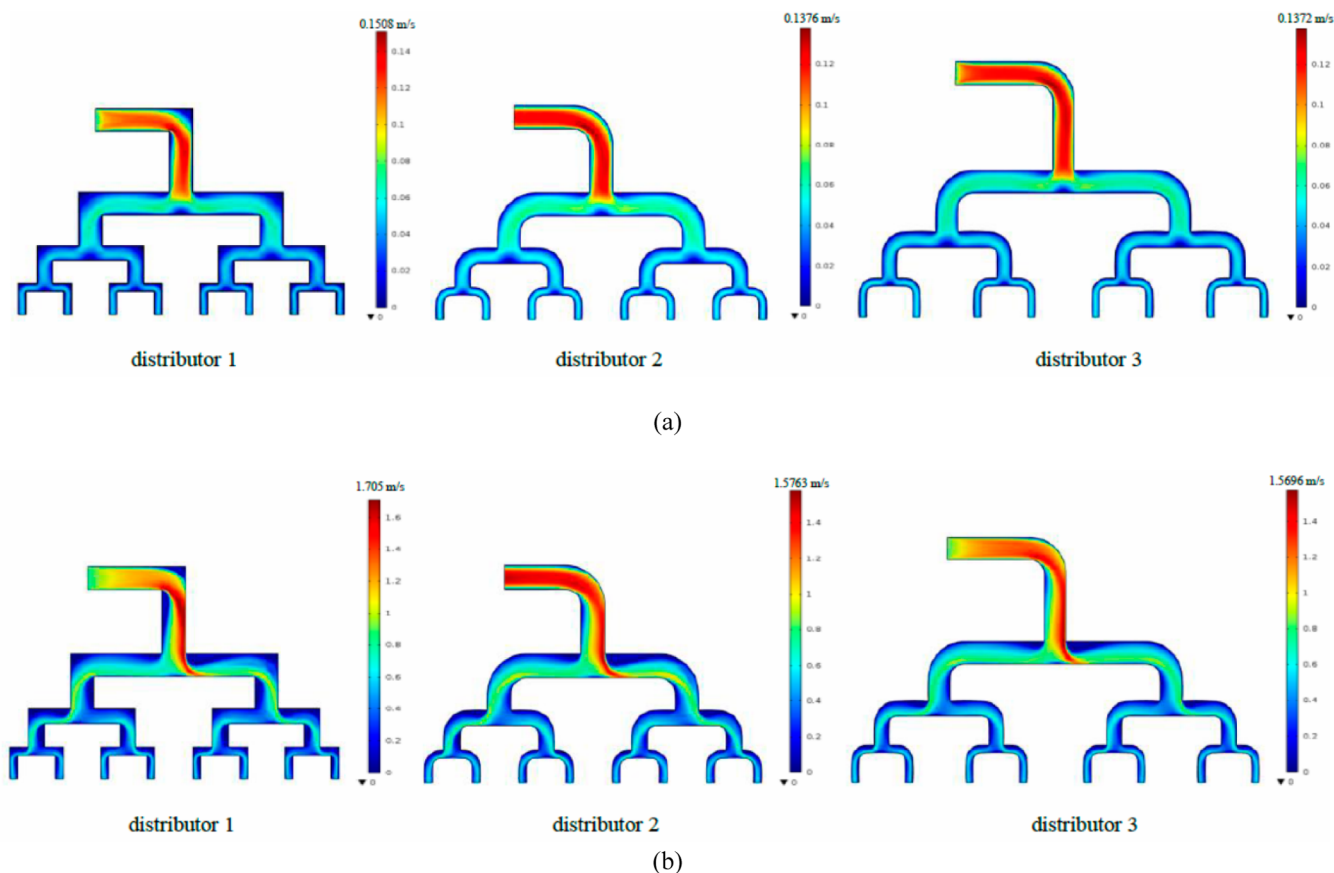


Figure 9. Contours of velocity magnitude at the central plane of distributors for two different Reynolds numbers: (a) $Re_{in} = 50$, (b) $Re_{in} = 600$.

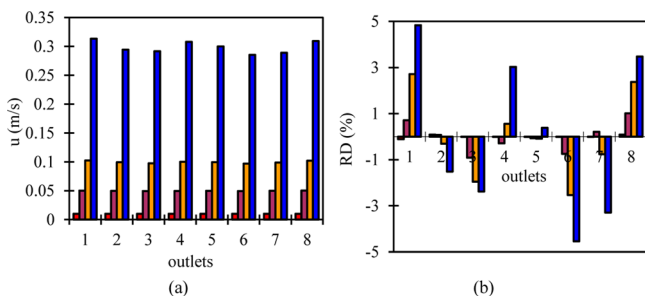


Figure 10. Velocity magnitude (a) and relative deviation (b) at the eight outlets of distributor 2 for different Reynolds numbers: red, $Re_{in} = 20$; purple, $Re_{in} = 100$; orange, $Re_{in} = 200$; blue, $Re_{in} = 600$.

The value of SD for distributor 3 does not exceed 2.5% when the inlet Reynolds number is less than 1000. For the same inlet Reynolds number, the value of SD for distributor 3 is smaller than the values for distributors 1 and 2, indicating that the fluid distribution in distributor 3 is better. For most inlet Reynolds numbers, the value of SD for distributor 2 is less than 4%, and is lower than that for distributor 1.

For distributors 1 and 2, the value of l_2 in each zone decreases slightly when the elbow structure changes from right angle to circular arc in the rounding process. Nevertheless, this rounding process is beneficial to reduce the variation degree of the flow direction especially at high Reynolds numbers. The value of l_2 in the i th zone ($i = 1, 2, 3$) of the distributor should satisfy the following equation for ensuring the fully developed laminar flow:⁴⁶

$$l_{2,i} \geq 0.09Re_{in,i}d_{e,i} \quad (11)$$

The above equation is usually applied to evaluate the inlet effect of the channels. Here, we use it to approximately determine the critical length for the fully developed laminar flow in each zone of the distributor. Figure 11 shows the effect of the inlet Reynolds number in zone 1 on the minimum theoretical l_2 in zones 1–3 for fully developed laminar flow. It can be seen that the minimum theoretical l_2 in different zones increases with the increase of the inlet Reynolds number in zone 1. If the data from Figure 11 and

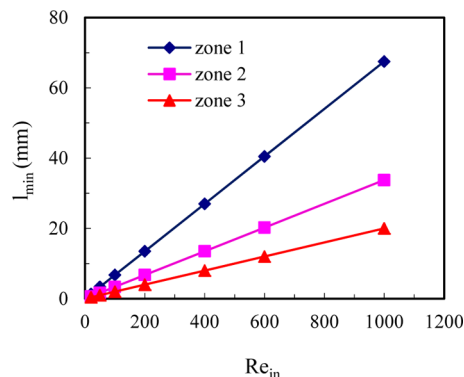


Figure 11. Effect of the inlet Reynolds number in zone 1 on the minimum theoretical l_2 in zones 1–3 of distributor for the fully developed laminar flow.

from Table 1 are compared, it can be seen that the value of l_2 is not large enough for fully developed laminar flow for these distributors at most of the inlet Reynolds numbers. In terms of space, the elbows are not symmetrical (if considered individually),

thus they cannot ensure fluid uniformity at the outlets of distributor under arbitrary flow rate condition. It can be concluded that both longer l_2 and lower flow rate are beneficial for obtaining a fully developed laminar flow in each zone of the distributor and hence for the improvement of the flow uniformity at the distributor outlets and in subsequent parallel microchannels.

In addition to the fluid distribution, pressure drop in these distributors is investigated. As expected, pressure drop in distributor 2 is much lower than that in distributors 1 and 3 (Figure 12). This tendency is especially pronounced at high

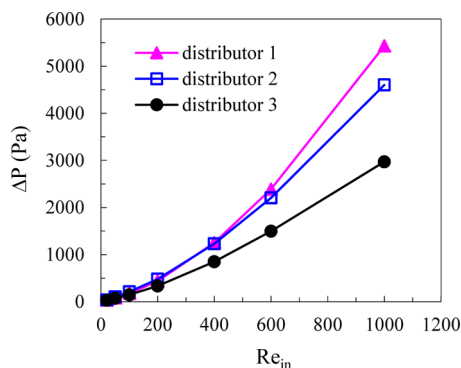


Figure 12. Pressure drop in different distributors.

Reynolds numbers ($Re_{in} > 600$). The circular arc structures in the elbows reduce the sharp change of the flow direction, and thus, significantly reduce the pressure drop as compared to the right angle structures. Considering both important factors, that is, fluid distribution performance and pressure drop, distributor 2 is considered to be the best choice for the ASMC design.

4.2. Mixing Efficiency in Multichannel Micromixers and ASMC Effect. The multichannel micromixer designs are suggested on the basis of the performed analysis of single microchannels and constructal distributors. In particular, distributor 2, and its axisymmetrical structure with eight vertical outlets whose shape and size correspond to those of the lateral inlets of single microchannels, are used as two distributors for liquids B and A, respectively. Eight microchannels are obtained from the duplication of a straight microchannel with a small lateral inlet, and then these microchannels are used as the parallel microchannels for the multichannel micromixer (cf., Figure 1). The microchannel with four zigzags is also used for the duplication. In this way, two multichannel micromixers are proposed: multichannel micromixer 1 with straight channels and multichannel micromixer 2 with zigzag channels. These two microchannels are chosen for the duplication because they have relatively high mixing performance and the pressure drop is low. The mean mixing efficiency and the energy dissipation in the suggested two multichannel micromixers are also investigated on the basis of numerical simulations.

The mean mixing efficiency in the multichannel micromixer (α_m) and ASMC effect (E) can be evaluated on the basis of the following expressions:

$$\alpha_m = \frac{\sum_{i=1}^8 (Q_i \cdot \alpha_i)}{Q_t} = \frac{\sum_{i=1}^8 (Q_i \cdot \alpha_i)}{Q_A + Q_B} \quad (12)$$

$$E = \frac{\alpha_m - \alpha_s}{\alpha_s} \times 100\% \quad (13)$$

where E is the relative deviation between the mean mixing efficiency of the parallel microchannels in the multichannel

micromixer (α_m) and the mixing efficiency of a single microchannel (α_s) evaluated for even distribution between the channels and at the same Reynolds number. When the mean mixing performance in the multichannel micromixer is lower than that in a single microchannel, E is less than 0. For the same grid size as applied for single microchannel simulations presented above, the number of grid nodes for the whole multichannel micromixer would be about 50 times higher than for a single microchannel. It is very difficult to simulate the whole multichannel micromixer with such a huge amount of grid nodes. In view of the computer memory and simulation time limitations, we consider the whole multichannel micromixer as a combination of two main parts: the distributor part and the microchannel part. Furthermore, the effect of the connectors and the collecting chamber on the fluid distribution is neglected.

First, the fluid distribution in the two distributors for the liquids A and B was studied, and the velocity values at the outlets of the distributors are used as the inlet velocities for the corresponding microchannels. Afterward, the mixing performance in each microchannel of the multichannel micromixer is simulated. Finally, the mean mixing quality in the multichannel micromixer and the ASMC effect can be determined.

Figure 13 shows the mean mixing efficiency in these multichannel micromixers and the corresponding ASMC effect.

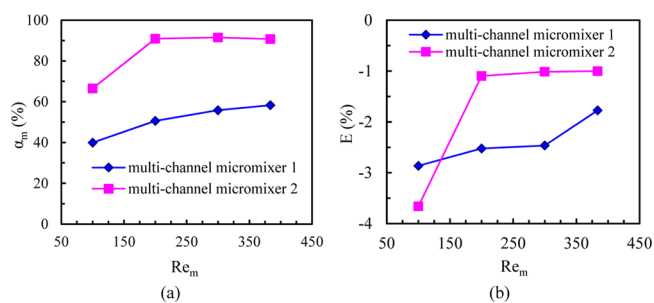


Figure 13. Mean mixing efficiency in the multichannel micromixers (a) and the ASMC effect (b).

It can be seen that the ASMC effect is not less than -4% when the mean Reynolds number of parallel microchannels in the multichannel micromixer is below 400. Thus, the mixing performance in these multichannel micromixers only slightly drops due to the insignificant maldistribution in the distributors, and the mean mixing performance in the multichannel micromixers can nearly reach the value of ideal single microchannels. This is due to the excellent fluid distribution performance in the constructal distributors, where the value of SD is smaller than 4%. Moreover, the ASMC effect does not decrease with increasing mean Reynolds number of parallel microchannels, which further demonstrates the advantages of these kinds of constructal distributors for ASMC.

We also analyze the mechanical energy dissipated in the two main parts of the multichannel micromixer (φ_t) and the ratio of the energy dissipated in the two distributors to the energy dissipated in the main parts (R). The pressure drop in the distributor comprises four constituents in different zones (shown in Figure 7c), where the energy dissipation occurs simultaneously. Therefore, the energy dissipation in the distributor (φ_d) can be calculated by the following equations:

$$\Delta P_d = \sum_{i=1}^4 \Delta P_i \quad (14)$$

$$\varphi_d = Q_1 \Delta P_1 + \sum_{j=1}^2 Q_{2,j} \Delta P_{2,j} + \sum_{j=1}^4 Q_{3,j} \Delta P_{3,j} + \sum_{j=1}^8 Q_{4,j} \Delta P_{4,j} \quad (15)$$

To simplify the calculation, an assumption is made that the fluid flow can be equally distributed in the distributors, so that the equations can further be transformed as follows:

$$Q_1 = 2Q_2 = 4Q_3 = 8Q_4 \quad (16)$$

$$\begin{aligned} \varphi_d &= Q_1 \Delta P_1 + 2Q_2 \Delta P_2 + 4Q_3 \Delta P_3 + 8Q_4 \Delta P_4 \\ &= Q_1 (\Delta P_1 + \Delta P_2 + \Delta P_3 + \Delta P_4) = Q_1 \Delta P_d \end{aligned} \quad (17)$$

φ_t and R can be calculated by the following equations:

$$\begin{aligned} \varphi_t &= \varphi_{d,1} + \varphi_{d,2} + 8\varphi_s \\ &= Q_1 (\Delta P_{d,1} + \Delta P_{d,2}) + \frac{2Q_1}{8} \times \Delta P_s \times 8 \\ &= Q_1 (\Delta P_{d,1} + \Delta P_{d,2} + 2\Delta P_s) \end{aligned} \quad (18)$$

$$R = \frac{\varphi_{d,1} + \varphi_{d,2}}{\varphi_{d,1} + \varphi_{d,2} + 8\varphi_s} = \frac{\Delta P_{d,1} + \Delta P_{d,2}}{\Delta P_{d,1} + \Delta P_{d,2} + 2\Delta P_s} \quad (19)$$

Figure 14 shows the effect of the inlet Reynolds number of the distributors on φ_t and R . It can be seen that the energy

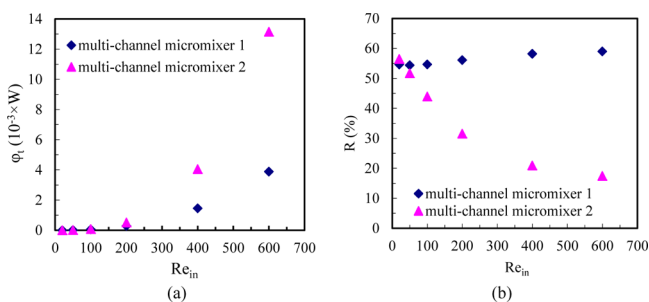


Figure 14. Energy dissipated in the main parts of the multichannel micromixer (a), and ratio of the energy dissipation in two distributors to that in the main parts (b).

dissipation in the multichannel micromixer 2 becomes obviously higher than that in the multichannel micromixer 1 as the inlet Reynolds number increases. In addition, the value of R is about the same for the multichannel micromixer 1. Nevertheless, it decreases drastically with increasing inlet Reynolds number for the multichannel micromixer 2, in which much higher mixing efficiency can be obtained as compared to micromixer 1. These results indicate that the energy dissipation in the distributors is relatively small when the mixing efficiency in the multichannel micromixer is high, and the mixing performance and the energy dissipation should be accounted for simultaneously when choosing the proper multichannel micromixer for a given process. At the same time, the specific energy dissipation in the multichannel micromixer ($\sigma = \varphi_t / \rho V$) is also evaluated on the basis of the data from Figure 14a, and is found to be in the range of 0.016–93 W/kg. As compared to other traditional mixers applied in industry, the specific energy dissipation in the multichannel micromixer is similar to that in batch reactors and much lower than that in

static mixers.^{49,50} Nevertheless, excellent mixing performance, small system volume, and fast assembly starting from single microchannels show the potential application of the multi-channel micromixers.

4.3. Design Procedure for Multichannel Micromixers.

The microchannel mixers are usually used as reactors for fast liquid reaction processes, in which the mixing performance has significant influence on the reaction conversion and product yield.⁵¹ On the basis of the above discussion, the design procedure for multichannel micromixers can be summarized as follows: Step 1, single microchannel designs are suggested according to the requirement of the mixing process. For example, if the reaction system is extremely fast, the microchannels with high mixing efficiencies should be chosen even when resulting in higher energy dissipation. Step 2, the effect of the flow ratio of two feeds on mixing and reaction is evaluated by simulations or experiments. If this effect is obvious, the distributors for the arrangements of single microchannels should be carefully selected to ensure an equal distribution of these two feeds. Step 3, the multichannel micromixers are designed on the basis of the previous two steps. The mixing performance and specific energy dissipation in the multichannel micromixers should be estimated and further compared to those in other mixers. For similar mixing efficiency, the mixers with lower specific energy dissipation should be preferred. Step 4, the throughput in multichannel micromixers can further be enhanced by increasing the number of parallel microchannels or by increasing the number of plates to form a stack.⁵²

5. CONCLUSIONS

The liquid mixing process in microchannel arrangements is investigated numerically. Single microchannels are designed for the assembly of multichannel micromixers, and the effects of some design parameters, such as the shape and size of lateral inlet and the form of mixing channel, on the mixing performance are studied. It is found that the decrease in the size of the lateral inlet can improve the mixing performance in microchannels, especially at relatively high Reynolds numbers. The mixing process in the zigzag-form microchannels is determined by different mixing mechanisms including molecular diffusion, convection, and chaotic advection, depending on the Reynolds number value. As the Reynolds number increases, the mixing in the zigzag-form microchannels is enhanced dramatically as compared to the straight microchannels, due to the convection and the chaotic advection. Under proper operational conditions, the mixing process in the zigzag-form microchannels can be almost completed ($\alpha = 98\%$). Nevertheless, the zigzag-form structures result in a much higher pressure drop as compared to the straight channels when $Re > 100$, and this effect becomes even more pronounced as the number of zigzags increases.

Flat constructal distributors are proposed for the arrangements of single microchannels, and their fluid distribution is characterized. The distance between the elbow and the closest split point is a key factor that influences the performance of distributors, and the rounding of the elbow can significantly reduce the pressure drop. For the optimized distributor, the standard deviation from the perfectly even distribution does not exceed 4% while keeping the pressure drop low.

Two multichannel micromixer designs are suggested on the basis of optimized single microchannels and distributors, and their mixing performance is also studied numerically. The results show that the mixing performance in these two multichannel micromixers can almost maintain the same value

as that in a single microchannel (E is not lower than -4%), which is attributed to the excellent fluid distribution performance in the constructal distributors. The energy dissipation in the main parts of the multichannel micromixer and the ratio of the energy dissipated in the distributors to that dissipated in the main parts of the multichannel micromixer are also estimated. The energy dissipation in the distributors is relatively small when the mixing efficiency in the multichannel micromixer is high. The mixing performance and the energy dissipation should be considered simultaneously when choosing the proper multichannel micromixer for a given process. The specific energy dissipation in the multichannel micromixer is in the range of $0.016\text{--}93\text{ W/kg}$, which is similar to the range in batch reactors and much lower than that in static mixers.

Finally, the design procedure for multichannel micromixers is proposed. These micromixers demonstrate excellent mixing performance, small system volume, and fast assembly starting from single microchannels, by application of the numbering-up method.

AUTHOR INFORMATION

Corresponding Author

*Tel.: +49-5251-60-2408. Fax: +49-5251-60-3522. E-mail: eugen.kenig@upb.de.

Notes

The authors declare no competing financial interest.

ACKNOWLEDGMENTS

Y.S. is grateful to the Alexander von Humboldt Foundation for financial support.

NOMENCLATURE

c = concentration of tracer in liquid, mol/m^3
 c_i = concentration of tracer at sampling point i , mol/m^3
 c_{max} = largest concentration of tracer in liquid, mol/m^3
 \bar{c}_M = optimal mixing concentration of the tracer when the mixing process is totally completed, mol/m^3
 d_e = hydraulic diameter of microchannel, m
 $d_{e,i}$ = hydraulic diameter of the elbow channel in the i th zone of the distributor, m
 D = diffusivity, m^2/s
 E = relative deviation between the mean mixing efficiency of the parallel microchannels in the multichannel micromixer and the mixing quality of a single microchannel
 h = width of microchannel, m
 l = length of microchannel, m
 l_1 = distance between the inlet and the elbow in different zones, m
 l_2 = distance between the elbow and the closest split point in different zones, m
 $l_{2,i}$ = distance between the elbow and the closest split point in the i th ($i = 1, 2, 3$) zone of the distributor, m
 l_m = distance between the inlet junction and the monitoring cross-section of the microchannel, m
 l_{min} = minimum theoretical length of l_2 , m
 n = number of sampling points inside the monitoring cross-section
 p = pressure, Pa
 Pe_Δ = grid Peclet number
 ΔP = pressure drop, Pa
 ΔP_d = pressure drop in distributor, Pa
 ΔP_s = pressure drop in a single microchannel, Pa
 $\Delta P_{d,k}$ = pressure drop in the k th distributors ($k = 1, 2$) of the multichannel micromixer, Pa

ΔP_i = pressure drop in the i th ($i = 1, 2, 3, 4$) zone of the distributor, Pa

$\Delta P_{2,j}$ = pressure drop in the j th ($j = 1, 2$) channel in zone 2 of the distributor, Pa

$\Delta P_{3,j}$ = pressure drop in the j th ($j = 1, 2, 3, 4$) channel in zone 3 of the distributor, Pa, Pa

$\Delta P_{4,j}$ = pressure drop in the j th ($j = 1, 2, 3, 4, 5, 6, 7, 8$) channel in zone 4 of the distributor, Pa

Q_t = total volumetric flow rate, m^3/s

Q_A = volumetric flow rate of liquid A, m^3/s

Q_B = volumetric flow rate of liquid B, m^3/s

Q_i = volumetric flow rate in each channel in the i th ($i = 1, 2, 3, 4$) zone of the distributor, m^3/s

$Q_{2,j}$ = volumetric flow rate in the j th ($j = 1, 2$) channel in zone 2 of the distributor, m^3/s

$Q_{3,j}$ = volumetric flow rate in the j th ($j = 1, 2, 3, 4$) channel in zone 3 of the distributor, m^3/s

$Q_{4,j}$ = volumetric flow rate in the j th ($j = 1, 2, 3, 4, 5, 6, 7, 8$) channel in zone 4 of the distributor, m^3/s

R = ratio of the energy dissipated in distributors to that dissipated in the main parts

Re = Reynolds number

Re_{in} = inlet Reynolds number

$Re_{\text{in},i}$ = inlet Reynolds number in the elbow channel in the i th zone of the distributor

Re_m = mean Reynolds number of parallel microchannels in the multichannel micromixer

RD_i = relative deviation between the actual velocity magnitude at the i th ($i = 1, 2, 3, 4, 5, 6, 7, 8$) outlet and the average velocity value at the eight outlets of the distributor

S = area of cross-section, m^2

SD = standard deviation between the actual velocity magnitude at each outlet and the average velocity value at the eight outlets of the distributor

u = velocity vector, m/s

u_i = velocity magnitude at the i th ($i = 1, 2, 3, 4, 5, 6, 7, 8$) outlet of the distributor, m/s

U = velocity magnitude, m/s

u_m = average value of velocity magnitude at the eight outlets, m/s

V = volume of multichannel micromixer, m^3

Greek Letters

α = mixing efficiency

α_m = mean mixing efficiency of the parallel microchannels in the multichannel micromixer

α_s = mixing efficiency of a single microchannel

μ = viscosity of water, $\text{Pa}\cdot\text{s}$

$\Delta\chi$ = grid size, m

ρ = density of water, kg/m^3

ν = kinematic viscosity of water, $\text{m}^2\cdot\text{s}^{-1}$

$\varphi_{d,k}$ = energy dissipation in the k th distributors ($k = 1, 2$) of the multichannel micromixer, W

φ_s = energy dissipation in a single microchannel, W

φ_t = energy dissipated in the main parts of the multichannel micromixer including distributors and parallel microchannels, W

Φ = specific energy dissipation in multichannel micromixer, W/kg

Subscripts

d = distributor

in = inlet

s = single microchannel

REFERENCES

- (1) Palanisamy, B.; Paul, B. Continuous flow synthesis of ceria nanoparticles using static T-mixers. *Chem. Eng. Sci.* **2012**, *78*, 46–52.
- (2) Baldyga, J.; Orciuch, W. Barium sulphate precipitation in a pipe - an experimental study and CFD modelling. *Chem. Eng. Sci.* **2001**, *56*, 2435–2444.
- (3) Khan, S. A.; Jensen, K. F. Microfluidic synthesis of titania shells on colloidal silica. *Adv. Mater.* **2007**, *19*, 2556–2560.
- (4) Engelmann, U.; Schmidnaake, G. Influence of micromixing on the free-radical polymerization in a discontinuous process. *Macromol. Theory Simul.* **1994**, *3*, 855–883.
- (5) Bourne, J. R. Mixing on the Molecular Scale (Micromixing). *Chem. Eng. Sci.* **1983**, *38*, 5–8.
- (6) Giridhar, M.; Krishnaiah, K. The effect of micromixing and macromixing on enzyme reaction in a real Cstr. *Bioprocess Eng.* **1993**, *9*, 263–269.
- (7) Tamir, A. *Impinging-Stream Reactors: Fundamentals and Applications*; Elsevier: Amsterdam, 1994.
- (8) Chen, J. F.; Wang, Y. H.; Guo, F. Synthesis of Nanoparticles with Novel Technology: High-Gravity Reactive Precipitation. *Ind. Eng. Chem. Res.* **2000**, *39*, 948–954.
- (9) Visscher, F.; van der Schaaf, J.; Nijhuis, T. A.; Schouten, J. C. Rotating reactors - A review. *Chem. Eng. Res. Des.* **2013**, *91*, 1923–1940.
- (10) Liu, S. P.; Hrymak, A. N.; Wood, P. E. Laminar mixing of shear thinning fluids in a SMX static mixer. *Chem. Eng. Sci.* **2006**, *61*, 1753–1759.
- (11) Jin, H. D.; Garrison, A.; Tseng, T.; Paul, B. K.; Chang, C. H. High-rate synthesis of phosphine-stabilized undecagold nanoclusters using a multilayered micromixer. *Nanotechnology* **2010**, *21*, 445604.
- (12) Kochmann, N. *Transport Phenomena in Micro Process Engineering*; Springer: New York, 2007.
- (13) Hessel, V.; Kralisch, D.; Kockmann, N.; Noël, T.; Wang, Q. Novel process windows for enabling, speeding-up and uplifting chemistry. *ChemSusChem* **2013**, *6*, 746–789.
- (14) Newman, S. G.; Jensen, K. F. The role of flow in green chemistry and engineering. *Green Chem.* **2013**, *15*, 1456–1472.
- (15) Hessel, V.; Löwe, H. Microchemical engineering: Components, plant concepts user acceptance - Part I. *Chem. Eng. Technol.* **2003**, *26*, 13–24.
- (16) Liu, X. Y.; Jensen, K. F. Direct oxidative amidation of aromatic aldehydes using aqueous hydrogen peroxide in continuous flow microreactor systems. *Green Chem.* **2012**, *14*, 1471–1474.
- (17) Wang, K.; Lu, Y. C.; Shao, H. W.; Luo, G. S. Measuring Enthalpy of Fast Exothermic Reaction with Micro-Reactor-Based Capillary Calorimeter. *AIChE J.* **2010**, *56*, 1045–1052.
- (18) Su, Y. H.; Chen, G. W.; Yuan, Q. Ideal micromixing performance in packed microchannels. *Chem. Eng. Sci.* **2011**, *66*, 2912–2919.
- (19) Baek, J.; Allen, P. M.; Bawendi, M. G.; Jensen, K. F. Investigation of Indium Phosphide Nanocrystal Synthesis Using a High-Temperature and High-Pressure Continuous Flow Microreactor. *Angew. Chem., Int. Ed.* **2011**, *50*, 627–630.
- (20) Chasanis, P.; Brass, M.; Kenig, E. Y. Investigation of multicomponent mass transfer in liquid-liquid extraction systems at microscale. *Int. J. Heat Mass Transfer* **2010**, *53*, 3758–3763.
- (21) Noël, T.; Hessel, V. Membrane microreactors: gas-liquid reactions made easy. *ChemSusChem* **2013**, *6*, 405–407.
- (22) Ehrfeld, W.; Golbig, K.; Hessel, V.; Löwe, H.; Richter, T. Characterization of mixing in micromixers by a test reaction: Single mixing units and mixer arrays. *Ind. Eng. Chem. Res.* **1999**, *38*, 1075–1082.
- (23) Schönfeld, F.; Hessel, V.; Hofmann, C. An optimized split-and-recombine micro-mixer with uniform “chaotic” mixing. *Lab Chip* **2004**, *4*, 65–69.
- (24) Nagasawa, H.; Aoki, N.; Mae, K. Design of a new micromixer for instant mixing based on the collision of micro segments. *Chem. Eng. Technol.* **2005**, *28*, 324–330.
- (25) Kim, B. J.; Yoon, S. Y.; Lee, K. H.; Sung, H. J. Development of a microfluidic device for simultaneous mixing and pumping. *Exp. Fluids* **2009**, *46*, 85–95.
- (26) Noël, T.; Musacchio, A. J. Suzuki-Miyaura cross-coupling of heteroaryl halides and arylboronic acids in continuous flow. *Org. Lett.* **2011**, *13*, 5180–5183.
- (27) Shang, M.; Noël, T.; Wang, Q.; Hessel, V. Packed-bed microreactor for continuous-flow adipic acid synthesis from cyclohexene and hydrogen peroxide. *Chem. Eng. Technol.* **2013**, *36*, 1001–1009.
- (28) Engler, M.; Kockmann, N.; Kiefer, T.; Woias, P. Numerical and experimental investigations on liquid mixing in static micromixers. *Chem. Eng. J.* **2004**, *101*, 315–322.
- (29) Adeosun, J. T.; Lawal, A. Numerical and experimental studies of mixing characteristics in a T-junction microchannel using residence-time distribution. *Chem. Eng. Sci.* **2009**, *64*, 2422–2432.
- (30) Hong, C. H.; Choi, J. W.; Ahn, C. H. A novel in-plane passive microfluidic mixer with modified Tesla structures. *Lab Chip* **2004**, *4*, 109–113.
- (31) Chang, S.; Cho, Y. H. Static micromixers using alternating whirls and lamination. *J. Micromech. Microeng.* **2005**, *15*, 1397–1405.
- (32) Mengeaud, V.; Josserand, J.; Girault, H. H. Mixing processes in a zigzag microchannel: finite element simulations and optical study. *Anal. Chem.* **2002**, *74*, 4279–4286.
- (33) Ansari, M. A.; Kin, K. Y. A numerical study of mixing in a microchannel with circular mixing chambers. *AIChE J.* **2009**, *55*, 2217–2225.
- (34) Soleymani, A.; Kolehmainen, E.; Turunen, I. Numerical and experimental investigations of liquid mixing in T-type micromixers. *Chem. Eng. J.* **2008**, *135*, S219–S228.
- (35) Saber, M.; Commenge, J. M.; Falk, L. Microreactor numbering-up in multi-scale networks for industrial-scale applications: Impact of flow maldistribution on the reactor performances. *Chem. Eng. Sci.* **2010**, *65*, 372–379.
- (36) Commenge, J. M.; Falk, L.; Corriou, J. P.; Matlosz, M. Optimal design for flow uniformity in microchannel reactors. *AIChE J.* **2002**, *48*, 345–358.
- (37) Amador, C.; Gavrilidis, A.; Angeli, P. Flow distribution in different microreactor scale-out geometries and the effect of manufacturing tolerances and channel blockage. *Chem. Eng. J.* **2004**, *101*, 379–390.
- (38) Yue, J.; Boichot, R.; Luo, L.; Gonthier, Y.; Chen, G. W.; Yuan, Q. Flow distribution and mass transfer in a parallel microchannel contactor integrated with structural distributors. *AIChE J.* **2010**, *56*, 298–317.
- (39) Chen, Y. Z.; Su, Y. H.; Jiao, F. J.; Chen, G. W. A simple and efficient synthesis protocol for sulfonation of nitrobenzene under solvent-free conditions via a microreactor. *RSC Adv.* **2012**, *2*, 5637–5644.
- (40) COMSOL AB, Product information COMSOL Multiphysics 3.5; Stockholm, 2008.
- (41) Sullivan, S. P.; Akpa, B. S.; Matthews, S. M.; Fisher, A. C.; Gladden, L. F.; Johns, M. L. Simulation of miscible diffusive mixing in microchannels. *Sens. Actuator, B: Chem.* **2007**, *123*, 1142–1152.
- (42) Dean, W. R. Note on the motion of fluid in a curved pipe. *Philos. Mag.* **1927**, *4*, 208–223.
- (43) Su, Y. H.; Zhao, Y. C.; Chen, G. W.; Yuan, Q. Intensification of liquid-liquid two-phase mass transfer by gas agitation in a microchannel. *AIChE J.* **2009**, *55*, 1948–1958.
- (44) Jiang, F.; Drese, K. S.; Hardt, S.; Küpper, M.; Schönfeld, F. Helical Flows and Chaotic Mixing in Curved Micro Channels. *AIChE J.* **2004**, *50*, 2297–2305.
- (45) Sui, Y.; Teo, C. J.; Lee, P. S. Direct numerical simulation of fluid flow and heat transfer in periodic wavy channels with rectangular. *Int. J. Heat Mass Transfer* **2012**, *55*, 73–88.
- (46) Shah, R. K.; London, A. L. *Laminar Flow Forced Convection in Ducts*; Academic Press: New York, 1978.

(47) Dreher, S.; Kockmann, N.; Woias, P. Characterization of Laminar Transient Flow Regimes and Mixing in T-shaped Micromixers. *Heat Transfer Eng.* **2009**, *30*, 91–100.

(48) Rebrov, E. V.; Schouten, J. C.; de Croon, M. H. J. M. Single-phase fluid flow distribution and heat transfer in microstructured reactors. *Chem. Eng. Sci.* **2011**, *66*, 1374–1393.

(49) Cybulski, A.; Moulijn, J. A.; Sharma, M. M.; Sheldon, R. A. *Fine Chemicals Manufacture - Technology and Engineering*; Elsevier: Amsterdam, 2001.

(50) Merchuk, J. C.; Shai, R.; Wolf, D. Experimental study of copper extraction with LIX-64N by means of motionless mixers. *Ind. Eng. Chem. Res.* **1980**, *19*, 91–97.

(51) Hartman, R. L.; McMullen, J. P.; Jensen, K. F. Deciding whether to go with the flow: Evaluating the merits of flow reactors for synthesis. *Angew. Chem., Int. Ed.* **2011**, *50*, 7502–7519.

(52) Kölbl, A.; Kraut, M.; Schubert, K. On the scalability of microstructured mixing devices. *Chem. Eng. J.* **2010**, *160*, 865–872.